CO_2 Reduction Hot Paper

Deutsche Ausgabe: DOI: 10.1002/ange.201509800
Internationale Ausgabe: DOI: 10.1002/anie.201509800

Ultrathin Co_3O_4 Layers Realizing Optimized CO_2 Electroreduction to Formate

Shan Gao[+], Xingchen Jiao[+], Zhongti Sun, Wenhua Zhang, Yongfu Sun, Chengming Wang, Qitao Hu, Xiaolong Zu, Fan Yang, Shuyang Yang, Liang Liang, Ju Wu, and Yi Xie**

Abstract: *Electroreduction of CO_2 into hydrocarbons could contribute to alleviating energy crisis and global warming. However, conventional electrocatalysts usually suffer from low energetic efficiency and poor durability. Herein, atomic layers for transition-metal oxides are proposed to address these problems through offering an ultralarge fraction of active sites, high electronic conductivity, and superior structural stability. As a prototype, 1.72 and 3.51 nm thick Co_3O_4 layers were synthesized through a fast-heating strategy. The atomic thickness endowed Co_3O_4 with abundant active sites, ensuring a large CO_2 adsorption amount. The increased and more dispersed charge density near Fermi level allowed for enhanced electronic conductivity. The 1.72 nm thick Co_3O_4 layers showed over 1.5 and 20 times higher electrocatalytic activity than 3.51 nm thick Co_3O_4 layers and bulk counterpart, respectively. Also, 1.72 nm thick Co_3O_4 layers showed formate Faradaic efficiency of over 60 % in 20 h.*

Global warming and the energy crisis are two important issues we are facing in the 21st Century. Both problems are rooted in the unsustainable utilization of fossil fuels accompanied with release of greenhouse gas CO_2.[1a–c] In this regard, CO_2 reduction into useful fuels, powered by a renewable electricity source, could not only help to reduce CO_2 emission, but also decrease the energy shortage.[1b–d] Over the past three decades, researchers have evaluated lots of metals as electrodes for CO_2 reduction in aqueous solutions.[1a,2] While these metal electrodes show competent CO_2 electroreduction performances, they usually suffer from very high prices, limited availability, as well as rapid loss of CO_2 reduction activity,[1a] which seriously hinder their large-scale practical applications. To address these issues, several naturally abundant and chemically stable transition-metal oxides have been recently explored as potential CO_2 electroreduction catalysts to replace the expensive and easily deactivated metals.[3] Among these materials, the spinel-type oxide of Co_3O_4 seems to be one of the most competitive candidates for electrocatalytic CO_2 reduction. In addition to being environmental friendly, having low cost and an abundance of reserves, the Co_3O_4 adopts a normal spinel structure with Co^{2+} ions in tetrahedral interstices and Co^{3+} ions in octahedral interstices, in which the peculiar crystal structure enables it to be high environmental stability.[4] In spite of these advantages, the catalytic CO_2 reduction performance of Co_3O_4 is still far from satisfactory,[3a] which is primarily ascribed to the very low amount of active sites associated with poor electrical conductivity in previously fabricated Co_3O_4 catalysts. Henceforth, designing a suitable material with abundant active sites and high electrical conductivity holds the key to greatly promoting the electrocatalytic CO_2 reduction performances.

Herein, we construct an ideal model of transition-metal-oxide-based atomic layers, which possess abundant active sites and high electrical conductivity, hence showing promise for substantially promoting the CO_2 electroreduction. Taking the ultrathin Co_3O_4 layers as an example, the atomic thickness means the majority of the Co atoms are exposed on the surface, in which the surface Co atoms have lowered coordination number compared with interior atoms, as disclosed by X-ray absorption fine structure spectroscopy in our previously systematic studies.[5] Also, as revealed by pioneering research on TiO_2 and MgO, it was demonstrated that the low-coordinated surface metal cations of transition-metal oxides could serve as the main adsorption sites for CO_2 in the reduction processes.[6] In this case, the ultrahigh fraction of low-coordinated surface Co atoms may act as the potential active sites for efficiently adsorbing CO_2, hence fulfilling the prerequisite to perform the required reduction reactions. Moreover, as depicted by the density-functional-theory (DFT) calculations in Figure 1 A,B, it can clearly be seen that the ultrathin Co_3O_4 layer exhibits a remarkably higher density of states (DOS) at the conduction band edges than its bulk counterpart. In addition, from the partial charge density in Figure 1 C,D, the charge density around the conduction band edge in the ultrathin Co_3O_4 layer was increased noticeably and was more dispersive than in the bulk Co_3O_4. These changes should be beneficial for faster carrier transport to participate the CO_2 reduction reactions along the two-dimensional (2D) conducting channels.[7a] Furthermore, the ultrathin 2D layers are usually accompanied by structure distortion, demonstrated by our previous investigations,[5b,7b] which could help to decrease surface energy and hence ensure better structure stability. In addition, the quick electron transport along the 2D ultrathin layer allows for low corrosion rates and hence guarantees long-term durability in the aqueous electrolyte.[7b] Accordingly, to achieve

[*] S. Gao,[+] X. Jiao,[+] Z. Sun, Prof. W. Zhang, Prof. Y. Sun, Dr. C. Wang, Q. Hu, X. Zu, F. Yang, S. Yang, L. Liang, J. Wu, Prof. Y. Xie
Hefei National Laboratory for Physical Sciences at Microscale, Collaborative Innovation Center of Chemistry for Energy Materials
University of Science & Technology of China
Hefei, Anhui 230026 (P. R. China)
E-mail: yfsun@ustc.edu.cn
yxie@ustc.edu.cn

[+] These authors contributed equally to this work.

Supporting information for this article is available on the WWW under http://dx.doi.org/10.1002/anie.201509800.

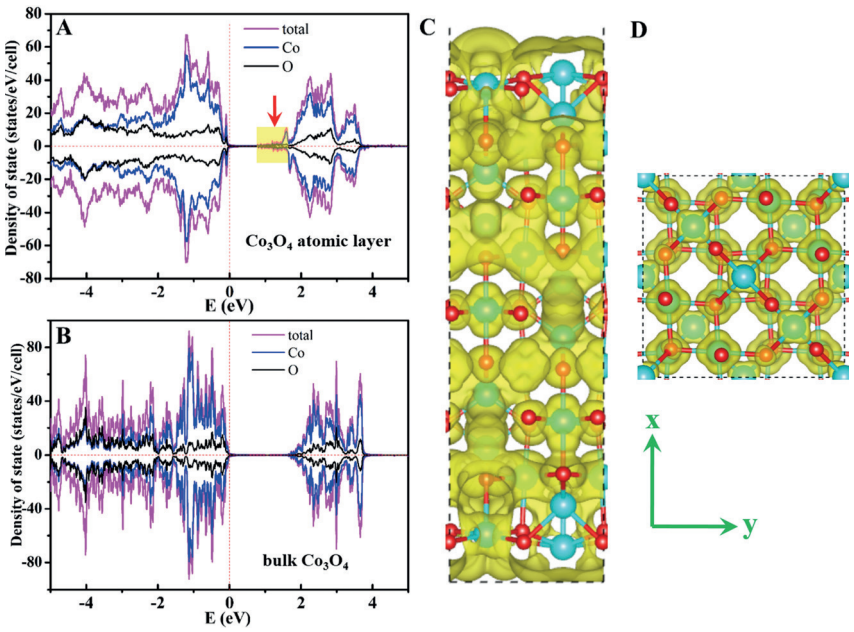

Figure 1. Density of state (DOS) and charge-density distribution. Calculated DOS for A) Co_3O_4 atomic layer slab with thickness of 1.72 nm and B) bulk Co_3O_4 slab. The yellow shaded parts represent the increased DOS at the conduction band edges of Co_3O_4 atomic layer. The partial charge density around the conduction band minimum of C) Co_3O_4 atomic layer slab and D) bulk Co_3O_4 slab, in which yellow refers to charge density contour with the isovalue of 0.0001 e/bohr^3. Cyan Co and red O atoms.

efficient and robust CO_2 electroreduction performances, it is crucially important to controllably synthesize Co_3O_4 atomic layers, whereas the strong in-plane bonds and the lack of intrinsic driving force for 2D anisotropic growth enable the fabrication of ultrathin Co_3O_4 layers to be a grant challenge.

To achieve this important goal, the ultrathin Co_3O_4 layers with average thickness of 1.72 nm were successfully fabricated by fast-heating the precursors of ultrathin $Co(CO_3)_{0.5}(OH)\cdot 0.11\,H_2O$ layers (Figure S1 in the Supporting Information), which were obtained via a controllable reaction between $Co(acac)_3$ and cetyltrimethyl ammonium bromide. The XRD pattern for the finally collected powder sample could be readily indexed to cubic Co_3O_4, corresponding to JCPDS card No. 78-1969 (Figure S3).[8] Meanwhile, the XPS spectra in Figure S4 A, B demonstrated the presence of elements Co and O, while no evident impurities were detected, illustrating the formation of pure Co_3O_4, which was further verified by the corresponding IR spectrum in Figure S4C.[4a] In addition, the blue-shifted Raman bands in Figure S4D, compared to the bulk counterpart, could be ascribed to the phonon confinement effect, and reasonably inferred the ultrathin thickness. TEM images of the products clearly revealed their 2D sheet-like structure with the sheet size larger than 500 nm (Figure 2 A), while their nearly transparent nature implied their ultrathin thickness, further verified by their atomic force microscopy (AFM) in Figure 1 C, D. HRTEM image in Figure 2 B revealed their [001] orientation, suggesting the formation of ultrathin Co_3O_4 layers with highly preferred [001] direction. The AFM image and the corresponding height profiles in Figure 1 C, D show the smooth 2D sheets with an average thickness of 1.72 nm. Therefore, all the aforementioned results strongly confirmed the successful synthesis of clean ultrathin Co_3O_4 layers with controllable thickness of 1.72 nm.

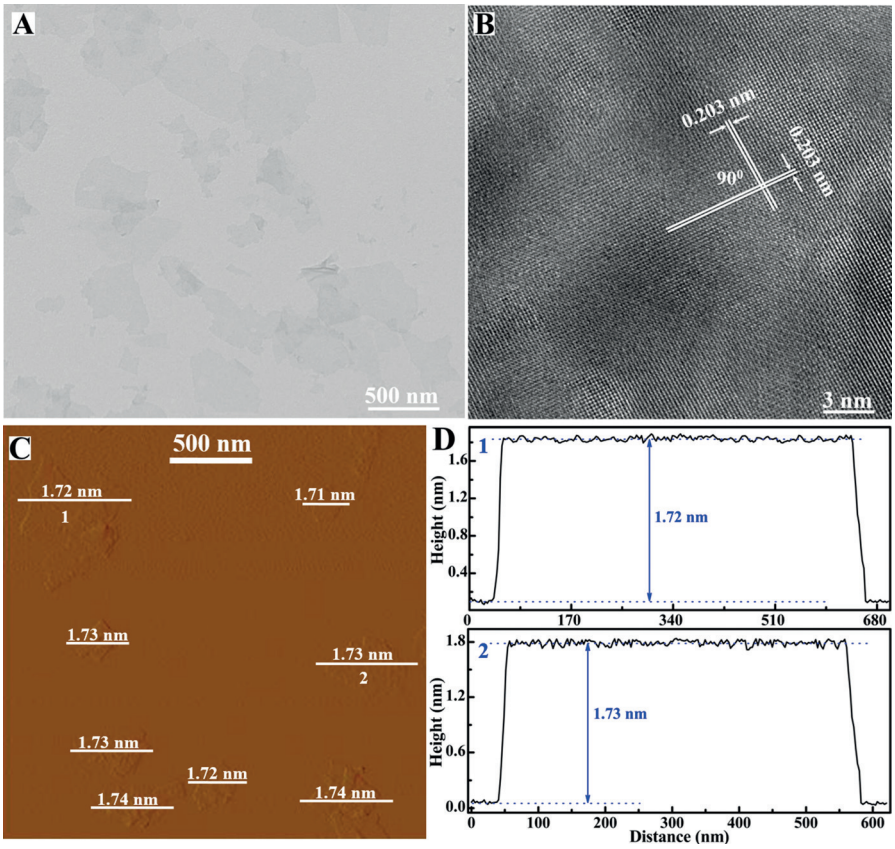

Figure 2. Characterizations for Co_3O_4 atomic layers with an average thickness of 1.72 nm. A) TEM image, B) HRTEM image, C) AFM image and D) the corresponding height profiles for Co_3O_4 atomic-layers with average thickness of 1.72 nm; the numbers 1 to 2 in (D) correspond to the numbers from 1 to 2 in (C).

To better study the CO_2 electroreduction properties, ultrathin Co_3O_4 layers with an average thickness of 3.51 nm were also fabricated through fast heating of the synthetic 3.51 nm thick $Co(CO_3)_{0.5}(OH)\cdot 0.11\,H_2O$ layers (Figure S2, S5, and S6), and were selected as a reference to compare the catalytic properties of the thinner layers.

Thanks to their ultrathin thickness, the Co_3O_4 atomic layers have an ultralarge fraction of coordinatively unsaturated surface atoms, which could serve as the catalytically active sites to trigger CO_2 reduction into energy-rich fuels. To verify the predictions, CO_2 electroreduction measurements were performed on the bulk Co_3O_4 (Figure S7) and the two Co_3O_4 atomic layers with thicknesses of 1.72 nm and 3.51 nm, respectively. As expected, bulk Co_3O_4 exhibited very poor electrocatalytic properties for CO_2 reduction over all the applied potentials. By contrast, the Co_3O_4 atomic layers gave clearly increased CO_2 reduction performances in comparison with the bulk counterpart, demonstrating the superior activity of the ultrathin 2D structure. For example, the 1.72 nm thick Co_3O_4 layers showed a current density of 0.68 mA cm^{-2} at −0.88 V versus the saturated calomel electrode (SCE), a value over 1.5 and 20 times higher than that of the 3.51 nm thick Co_3O_4 layers and bulk counterpart, respectively. To identify the reduction products, ^{1}H NMR spectroscopy was carried out to quantify the liquid products after 4 h electrolysis at each given potential. As displayed in Figure 3B, the 1.72 nm thick Co_3O_4 layers has the highest faradaic efficiency for formate production compared with the other two samples, especially in the low applied potentials. For instance, the 1.72 nm thick Co_3O_4 layers exhibited a maximum faradaic efficiency of 64.3% at −0.88 V vs. SCE, much higher than that of 3.51 nm thick Co_3O_4 layers (51.2%) and bulk counterpart (18.5%). Notably, the clearly promoted catalytic activity and Faradaic efficiency could be ascribed to the increased number of catalytically active sites. To verify this viewpoint, the electrochemically active surface area (ECSA) of these products was determined by measuring the double layer capacitance.[9a] Figure 3C revealed that the ECSA for the three samples gradually increased as the thickness decreased from bulk to 1.72 nm, confirming the close correlation between active sites and thickness of 2D structure. In addition, the ECSA-corrected linear sweep voltammetric (LSV) curves in Figure 3D illustrated the highest intrinsic catalytic activity of the 1.72 nm thick Co_3O_4 layers among the three samples, implying that the lowered thickness resulted in higher intrinsic activity. Moreover, it is noticeable that another crucial factor for evaluating CO_2 reduction performances is the durability under long-term electrolysis. Figure 3E,F show that the 1.72 nm thick Co_3O_4 layers did not show any obvious variation in the current densities and simultaneously their Faradaic efficiency for producing formate was always higher than 60% over 20 h, indicating their excellent stability. The 3.51 nm thick Co_3O_4 layers exhibited relatively poor long-term durability as well as gradually decreased Faradaic efficiency, while the bulk counterpart showed negligible CO_2 reduction activities.

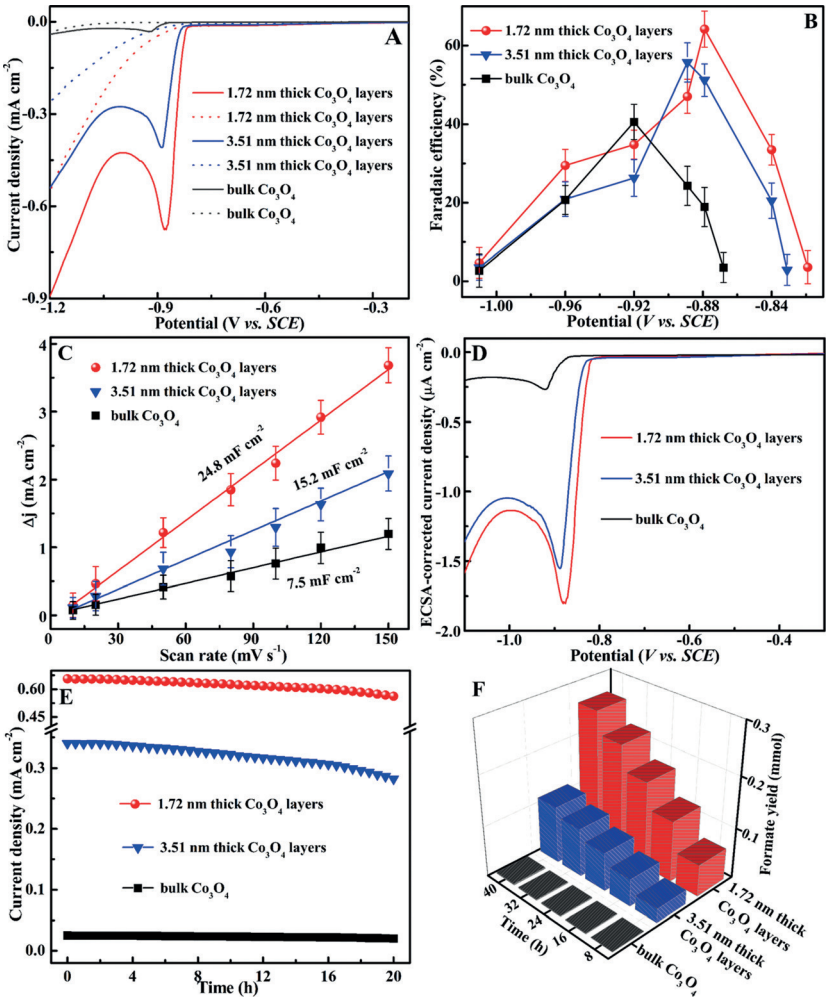

Figure 3. Electroreduction of CO_2 into formate by Co_3O_4 with different thicknesses. A) Linear sweep voltammetric curves in the CO_2 saturated (solid line) and N_2 saturated (dash line) 0.1 M $KHCO_3$ aqueous solution. B) Faradaic efficiencies for formate at each applied potentials for 4 h. C) Charging current density differences plotted against scan rates. D) ECSA-corrected current densities vs. applied potentials. E) Chrono-amperometry results and F) the corresponding formate yield at the potentials of −0.88 V versus SCE. Independently prepared electrodes evaluated under identical conditions in (F) show variability of less than 10% for the formate yield.

Of note, the clearly improved CO_2 electroreduction performances for the Co_3O_4 atomic layers could be attributed to their increased number of active sites, enhanced 2D electronic conductivity, as well as higher intrinsic catalytic activity. The ultrathin thickness down to atomic-scale endows the Co_3O_4 atomic layers with an ultra-large specific surface area, which could be verified by their greatly increased ECSA (Figure 3C). The abundant atoms exposed on the surface

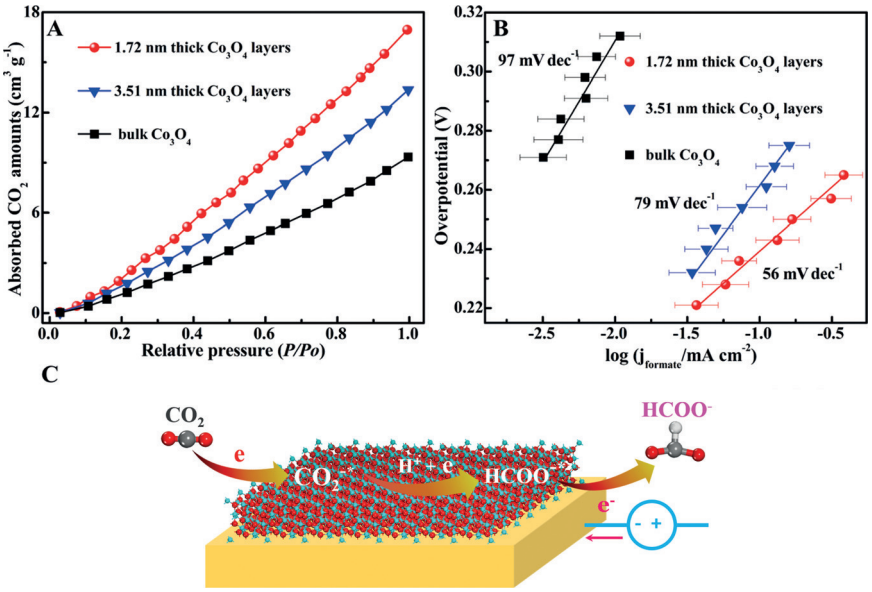

Figure 4. A) CO_2 adsorption isotherms and B) Tafel plots of formate for the Co_3O_4 atomic layers with different thicknesses. C) Scheme for the electroreduction CO_2 into formate on the Co_3O_4 atomic-layers.

could serve as the active sites to adsorb higher amounts of CO_2, confirmed by the CO_2 adsorption isotherms in Figure 4A, which shows the CO_2 adsorption amount increasing with the decreasing thickness of Co_3O_4. It is assumed that CO_2 adsorption is the prerequisite for it to participate the subsequent reactions and hence the largely increased CO_2 adsorption could continually provide raw materials for subsequent reduction reactions.[9b] Moreover, as revealed by the DFT calculations in Figure 1, the Co_3O_4 atomic layers have a clearly increased and more dispersed charge density compared with their bulk counterpart, which ensures higher electronic conductivity, further confirmed by the lowered interfacial transport resistance in electrochemical impedance spectra in Figure S8. In this case, the two-dimensional conducting paths allow for much faster electron transport in the Co_3O_4 atomic layers, and hence endows them with faster reduction kinetics, fairly correlating with their higher intrinsic activity illustrated by the ECSA-corrected LSV curves (Figure 3D). The Tafel slope, is an inherent property of electrocatalysts that is determined by the rate-limiting step. Figure 4B clearly reveals that both the 1.72 and 3.51 nm thick Co_3O_4 layers have a Tafel slope close to 59 mV dec^{-1}, while the bulk counterpart shows one close to 118 mV dec^{-1}. This indicates that the Co_3O_4 atomic layers and bulk counterpart undergo different CO_2 reduction mechanisms, in which the atomic layers probably exhibit a fast $1e^-$ pre-equilibrium transfer to form $CO_2^{\bullet-}$ prior to a chemical H^+ transfer step (Figure 4C), while the bulk Co_3O_4 proceeds an initial rate-limiting $1e^-$ transfer from CO_2 to $CO_2^{\bullet-}$ that needs very high overpotentials (Figure 3A,B).[1a,b,10] This could be a result of the ultrahigh fraction of surface atoms in the Co_3O_4 atomic layers, in which the low coordination number endows them with many dangling bonds that ensure a higher intrinsic catalytic activity, verified by the ECSA-corrected linear sweep voltammetric curves in Figure 3D. Thus, the abundant surface atoms with higher intrinsic activity could serve as the highly active sites to stabilize the rate-determining $CO_2^{\bullet-}$ intermediate, which helps to lower the rate-limiting activation energy barrier and hence remarkably increase the catalytic activity.

In conclusion, atomic layers for transition-metal oxides have been put forward to achieve efficient and robust CO_2 elecrtoreduction through offering an ultralarge fraction of active sites, high electronic conductivity, and superior structural stability. As an example, Co_3O_4 atomic layers with thickness of 1.72 and 3.51 nm were successfully synthesized through fast-heating the respective precursors of ultrathin $Co(CO_3)_{0.5}(OH)\cdot 0.11\,H_2O$ layers. ECSA investigations and adsorption isotherms demonstrated that the ultrathin Co_3O_4 layers have far more active sites and hence could adsorb higher amounts of CO_2, necessary for the subsequent reduction reactions. DFT calculations revealed that the ultrathin Co_3O_4 layers had a more dispersed charge density, which was beneficial for increased electronic conductivity confirmed by the electrochemical impedance spectra. ECSA-corrected LSV curves illustrated that the low-coordinated surface Co atoms confined in atomic layers endowed them with higher intrinsic activity, while the atomic layers with ultra-large fraction of surface Co atoms underwent a distinct reduction mechanism by effectively stabilizing the $CO_2^{\bullet-}$ intermediate in comparison with bulk counterpart, indicated by their typical Tafel slopes. As a result, the 1.72 nm thick Co_3O_4 layers had a current density of 0.68 mA cm^{-2} at −0.88 V vs. SCE, over 1.5 and 20 times higher than that of the 3.51 nm thick Co_3O_4 layers and bulk counterpart, respectively. Also, the 1.72 nm thick Co_3O_4 layers displayed increased Faradaic efficiency and stability relative to the other two samples, showing a formate Faradaic efficiency of over 60 % in 20 h. Briefly, this work provides a promising lead for the development of efficient and robust catalysts for electrolytic fuel synthesis.

Acknowledgements

This work was financially supported by National Nature Science Foundation (21331005, 21422107, 21201157, 91422303, 11321503, U1532265), Program for New Century Excellent Talents in University (NCET-13-0546), Youth Innovation Promotion Association of CAS (CX2340000100), and the Fundamental Research Funds for the Central Universities No. WK2340000063. Supercomputing center of USTC is acknowledged for computational support.

Keywords: atomic layers · CO_2 electroreduction · cobalt oxide · formate

How to cite: *Angew. Chem. Int. Ed.* **2016**, *55*, 698–702
Angew. Chem. **2016**, *128*, 708–712

[1] a) Y. H. Chen, C. W. Li, M. W. Kanan, *J. Am. Chem. Soc.* **2012**, *134*, 19969–19972; b) C. W. Li, J. Ciston, M. W. Kanan, *Nature* **2014**, *508*, 504–507; c) B. A. Rosen, A. S. Khojin, M. R. Thorson, W. Zhu, D. T. Whipple, P. J. A. Kenis, R. I. Masel, *Science* **2011**, *334*, 643–644; d) B. Kumar, M. Asadi, D. Pisasale, S. S. Ray, B. A. Rosen, R. Haasch, J. Abiade, A. L. Yarin, A. S. Khojin, *Nat. Commun.* **2013**, *4*, 2819.

[2] a) W. L. Zhu, Y. J. Zhang, H. Y. Zhang, H. F. Lv, Q. Li, R. Michalsky, A. A. Peterson, S. H. Sun, *J. Am. Chem. Soc.* **2014**, *136*, 16132–16135; b) X. Q. Min, M. W. Kanan, *J. Am. Chem. Soc.* **2015**, *137*, 4701–4708; c) Y. Hori, C. G. Vayenas, R. E. White, M. E. Gamboa-Aldeco, *Mod. Aspects Electrochem.* **2008**, *42*, 89–189.

[3] a) X. F. Huang, T. C. Cao, M. C. Liu, G. H. Zhao, *J. Phys. Chem. C* **2013**, *117*, 26432–26440; b) T. Sekimoto, M. Deguchi, S. Yotsuhashi, Y. Yamada, T. Masui, A. Kuiamata, S. Yamakoshi, *Electrochem. Commun.* **2014**, *43*, 95–97; c) S. C. Ma, Y. C. Lan, G. M. J. Perez, S. Moniri, P. J. A. Kenis, *ChemSusChem* **2014**, *7*, 866–874.

[4] a) Y. F. Sun, S. Gao, F. C. Lei, J. W. Liu, L. Liang, Y. Xie, *Chem. Sci.* **2014**, *5*, 3976–3982; b) X. W. Xie, Y. Li, Z. Q. Liu, M. Haruta, W. J. Shen, *Nature* **2009**, *458*, 746–749.

[5] a) Y. F. Sun, Q. H. Liu, S. Gao, H. Cheng, F. C. Lei, Z. H. Sun, Y. Jiang, H. B. Su, S. Q. Wei, Y. Xie, *Nat. Commun.* **2013**, *4*, 2899; b) Y. F. Sun, Z. H. Sun, S. Gao, H. Cheng, Q. H. Liu, J. Y. Piao, T. Yao, C. Z. Wu, S. L. Hu, S. Q. Wei, Y. Xie, *Nat. Commun.* **2012**, *3*, 1057.

[6] a) M. Chiesa, E. Giamello, *Chem. Eur. J.* **2007**, *13*, 1261–1267; b) H. Y. He, P. Zapol, L. A. Curtiss, *J. Phys. Chem. C* **2010**, *114*, 21474–21481.

[7] a) F. C. Lei, Y. F. Sun, K. T. Liu, S. Gao, L. Liang, B. C. Pan, Y. Xie, *J. Am. Chem. Soc.* **2014**, *136*, 6826–6829; b) Y. F. Sun, H. Cheng, S. Gao, Z. H. Sun, Q. H. Liu, Q. Liu, F. C. Lei, T. Yao, J. F. He, S. Q. Wei, Y. Xie, *Angew. Chem. Int. Ed.* **2012**, *51*, 8727–8731; *Angew. Chem.* **2012**, *124*, 8857–8861.

[8] Y. Y. Liang, Y. G. Li, H. L. Wang, J. G. Zhou, J. Wang, T. Regier, H. J. Dai, *Nat. Mater.* **2011**, *10*, 780–786.

[9] a) L. Liang, H. Cheng, F. C. Lei, J. Han, S. Gao, C. M. Wang, Y. F. Sun, S. Qamar, S. Q. Wei, Y. Xie, *Angew. Chem. Int. Ed.* **2015**, *54*, 12004–12008; *Angew. Chem.* **2015**, *127*, 12172–12176; b) L. Liang, F. C. Lei, S. Gao, Y. F. Sun, X. C. Jiao, J. Wu, S. Qamar, Y. Xie, *Angew. Chem. Int. Ed.* **2015**, *54*, 13971–13974; *Angew. Chem.* **2015**, *127*, 14177—14180.

[10] a) C. W. Li, M. W. Kanan, *J. Am. Chem. Soc.* **2012**, *134*, 7231–7234; b) Y. H. Chen, M. W. Kanan, *J. Am. Chem. Soc.* **2012**, *134*, 1986–1989; c) M. Gattrell, N. Gupta, A. Co, *J. Electroanal. Chem.* **2006**, *594*, 1–19.

Received: October 19, 2015
Published online: November 24, 2015

